Pattern formation arising from interactions between Turing and wave instabilities

Lingfa Yang, Milos Dolnik,[a] Anatol M. Zhabotinsky, and Irving R. Epstein
Department of Chemistry and Center for Complex Systems, MS 015, Brandeis University, Waltham, Massachusetts 02454-9110

(Received 24 May 2002; accepted 24 July 2002)

We study pattern formation arising from the interaction of the stationary Turing and wave (oscillatory Turing) instabilities. Interaction and competition between these symmetry-breaking modes lead to the emergence of a large variety of spatiotemporal patterns, including modulated Turing structures, modulated standing waves, and combinations of Turing structures and spiral waves. Spatial resonances are obtained near codimension-two Turing-wave bifurcations. Far from bifurcation lines, we obtain inwardly propagating spiral waves with Turing spots at their tips. We demonstrate that the coexistence of Turing spots and traveling waves is a result of interaction between Turing and oscillatory modes, while the inwardly propagating waves (antispirals) do not require this interaction; they can arise from the wave instability combined with a negative group velocity. © *2002 American Institute of Physics.* [DOI: 10.1063/1.1507110]

I. INTRODUCTION

Studies of hydrodynamics, nonlinear optics, and reaction-diffusion systems have led to the characterization of three basic types of symmetry-breaking bifurcations responsible for the emergence of spatiotemporal patterns.[1] The classification of these bifurcations is based on linear stability analysis of a homogeneous state; the corresponding patterns are described in terms of a characteristic wave number k_0 and a characteristic frequency ω_0. The space-independent Hopf bifurcation breaks the temporal symmetry of a system and gives rise to oscillations that are uniform in space and periodic in time. The (stationary) Turing bifurcation breaks spatial symmetry, leading to the formation of patterns that are stationary in time and oscillatory in space. The wave (oscillatory Turing or finite-wavelength Hopf) bifurcation breaks both spatial and temporal symmetries, generating patterns that are oscillatory in space and time.

In reaction-diffusion systems, most studies have been devoted to traveling waves, which emerge in excitable systems near a Hopf bifurcation,[2–4] and to Turing structures arising from the Turing instability.[4–6] More recently, attention has turned toward patterns arising from the wave instability.[7–10] Although the individual bifurcations and the patterns emerging from them are well characterized, there have been fewer studies of the dynamics when symmetry-breaking instabilities interact. Pattern formation arising from interaction between Hopf and Turing modes, and their subharmonics near the codimension-two Hopf–Turing bifurcation point, have been analyzed in detail.[11–13] We have studied pattern formation near the Hopf and wave bifurcations and have observed a large variety of simple and complex traveling and standing wave patterns.[9,10] The interaction between the Turing and wave modes has not previously been studied. The wave instability plays an important role in pattern formation in many systems, such as binary fluid convection,[14] nematic liquid crystals,[1] and heterogeneous chemical,[15–18] and electrochemical systems.[19–21]

Standing waves have been found in an electrochemical system, in which mathematical modeling predicts Turing structures.[19,20] Recently, Turing structures and standing waves have been observed in the Belousov–Zhabotinsky (BZ) reaction in an Aerosol OT (AOT) microemulsion[22] under different conditions. Thus, one may expect that there are systems that possess a range of parameters where the Turing and wave instabilities interact. In this work we study the patterns that arise as a result of this interaction.

II. MODEL AND NUMERICAL METHODS

To study interactions between Turing and wave modes, we start from a reaction-diffusion model capable of generating Turing structures (a two-variable activator–inhibitor model for simplicity), and augment it with an additional reaction, in which the activator species X is reversibly transformed into an unreactive, rapidly diffusing species Z. Such a reaction has recently been suggested to explain patterns and waves observed in the BZ-AOT[22] system. Our equations take the form

$$\frac{\partial x}{\partial t} = D_x \nabla^2 x + f(x,y) - cx + dz, \tag{1}$$

$$\frac{\partial y}{\partial t} = D_y \nabla^2 y + g(x,y), \tag{2}$$

$$\frac{\partial z}{\partial t} = D_z \nabla^2 z + cx - dz, \tag{3}$$

where x, y, and z are dimensionless variables that correspond to the concentrations of the activator X, inhibitor Y, and unreactive species Z, respectively. D_x, D_y, D_z are their respec-

[a]Author to whom correspondence should be addressed. Electronic mail: dolnik@brandeis.edu

tive diffusion coefficients. The functions f and g are chemical kinetic terms, derived from a reaction scheme. In this paper, we select a simple abstract chemical scheme, the Brusselator model,[23] and a simplified model of a specific reaction, the two-variable Oregonator model.[24,25] The parameters c and d are rescaled rate constants for the reversible reaction in which the activator, X, is converted to an unreactive species, Z.

This additional reversible reaction is responsible for the emergence of the wave instability, which requires at least three variables.[5] The Turing instability can occur only if the autocatalytic species (activator) diffuses more slowly than the inhibitor. For the wave instability to arise in our model, the unreactive species must diffuse even faster than the inhibitor. Therefore, the diffusion coefficients are selected in our numerical investigations of Eqs. (1)–(3), so that $D_x < D_y < D_z$.

The reaction-diffusion equations were solved numerically in one and two spatial dimensions using a finite-difference approximation for the spatial derivatives and an explicit Euler method for the time integration. Neumann (zero-flux) boundary conditions were employed in most of the calculations. The first variable is displayed in space–time plots, and its value is quantified by gray levels; white corresponds to the maximum value and black to the minimum. Unless stated otherwise, random initial conditions were used.

III. EXTENDED BRUSSELATOR MODEL

For the Brusselator model,[23] the kinetic terms in (1)–(2) are

$$f(x,y) = a - (1+b)u + u^2 v, \tag{4}$$

$$g(x,y) = bu - u^2 v, \tag{5}$$

where parameters a, b, c, and d are rescaled kinetic parameters. The steady state of the model (1)–(3) is $(x_{ss}, y_{ss}, z_{ss}) = (a, b/a, ac/d)$. Linear stability analysis yields the bifurcation diagram shown in Fig. 1. The Hopf bifurcation line [$\mathrm{Im}(\lambda) \neq 0$, $\mathrm{Re}(\lambda) = 0$ at $k = 0$], the wave bifurcation line [$\mathrm{Im}(\lambda) \neq 0$, $\mathrm{Re}(\lambda) = 0$ at $k = k_w \neq 0$], and the Turing bifurcation line [$\mathrm{Im}(\lambda) = 0$, $\mathrm{Re}(\lambda) = 0$ at $k = k_T \neq 0$] intersect at two codimension-two bifurcation points, the Turing–Hopf bifurcation point and the Turing-wave bifurcation point [Fig. 1(a)]. The bifurcation lines separate the parametric space into six distinct domains. In domain I, located below all three bifurcation lines, the steady state is the only stable solution of the system. Domains II and III are regions of pure wave and pure Turing instabilities, respectively. In domain IV, both wave and Turing instabilities occur, and in domain V, the wave and Hopf modes arise. When the parameters correspond to domain VI, which is located above all three bifurcation lines, all three instabilities occur. Figure 1(b) shows a series of dispersion relations with two peaks (wave and Turing) in the most positive (least negative) real part of the eigenvalue.

One-dimensional numerical solutions with zero-flux boundary conditions reveal that Turing structures are stable in the pure Turing instability domain III as well as in regions of domains IV and VI far from the codimension-two points.

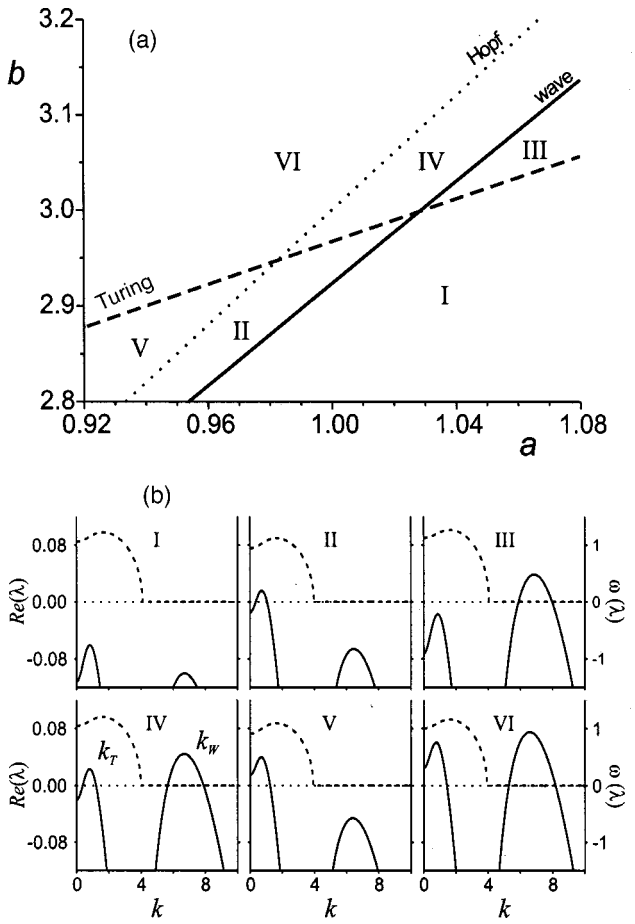

FIG. 1. Bifurcation diagram for the extended Brusselator model. (a) Three bifurcation lines separate the parameter space into six domains with dispersion relations shown in (b). Parameters: $(D_u, D_v, D_w) = (0.01, 0.1, 1)$, $c = d = 1$, $(a,b) = (1.04, 2.90)$ (I); (0.96,2.85) (II); (1.08,3.10) (III); (1.03,3.05) (IV); (0.94,2.85) (V); and (1.00,3.05) (VI). Solid line: real part of the most positive eigenvalue; dashed line: imaginary part of complex pair of eigenvalues.

However, if the parameters are selected close to the wave instability line or to the codimension-two point, the pure stationary Turing structures become modulated with a wavelength several times longer than that of the Turing structures. This behavior indicates that nonlinear effects arising from the interaction between the Turing and wave modes cause the pure Turing mode to lose its stability before the wave bifurcation occurs. Figure 2 shows an example of how modulated Turing structures develop from a standing wave pattern. First, the initial unstable standing wave gives way to an almost uniform steady state [Fig. 2(a)], which is gradually converted into a Turing pattern [Fig. 2(b)]. This pattern remains almost unchanged for a significant period of time [Fig. 2(c)], after which modulation, first by standing and then by traveling waves, becomes apparent [Fig. 2(d)]. The final stable state of modulated Turing structures is shown in Fig. 2(e). The wavelength of the traveling waves that modulate the Turing structure is identical to the wavelength of the initial standing waves. Turing structures modulated by traveling waves are also typical solutions of our one-dimensional system in domain IV near the codimension-two point.

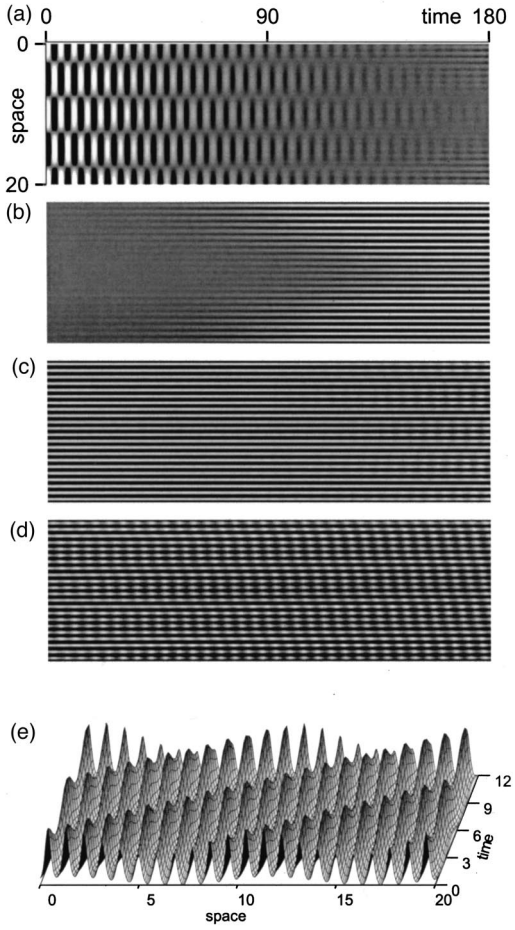

FIG. 2. Evolution of modulated Turing structures in the extended Brusselator model from initial pattern of pure standing waves in a one-dimensional system with periodic boundary conditions. Parameters: $(a,b)=(1.08,3.10)$, system length $L=20$. Values of x are quantified with gray levels; white corresponds to maximum and black to minimum. (a)–(c) Consecutive space–time plots of transient patterns; (d) space–time plot from 700 to 880 time units. (e) Stable pattern of modulated Turing structures. Vertical axis displays the value of x.

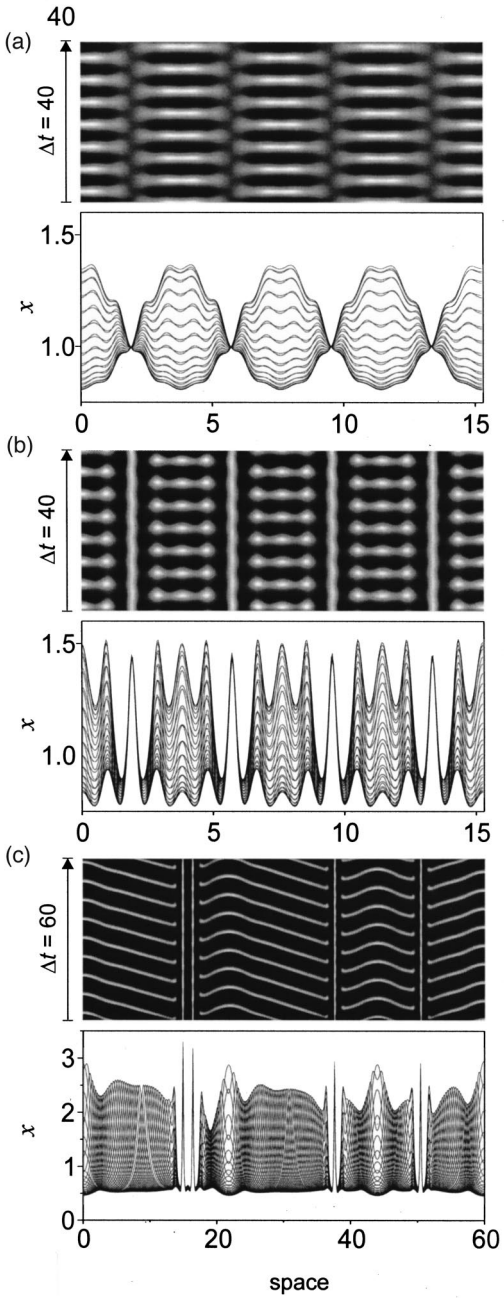

FIG. 3. Stable modulated standing waves and localized patterns in a one-dimensional Brusselator system with zero-flux boundary conditions and random initial conditions. Top panels show space–time plots; bottom panels show overlays of consecutive profiles for one full period of local oscillation. (a), (b) Modulated standing waves, $(a,b)=(1.03,3.05)$, $L=15.3$. (c) Localized Turing structures surrounded by traveling waves, $(a,b)=(0.92,3.20)$, $L=60$.

Standing waves, arising from the wave instability, have a characteristic wavelength λ_w. When this wavelength matches the length of the system L, i.e., when $L\approx n(\lambda_w/2)$, where n is a positive integer, the standing waves are stable in the pure wave instability domain II. Otherwise, a mixed pattern of standing (near the boundary) and traveling (in the bulk) waves arises.

The presence of the Turing mode and its interaction with the wave mode may result in modulation of the standing waves. As can be seen from the dispersion curves, patterns arising from the Turing and wave instabilities have quite different wavelengths. The wavelength of pure standing waves, λ_w, is significantly longer than that of Turing structures, λ_T. When the ratio λ_w/λ_T is close to an integer, the two emerging instabilities interact to produce patterns with characteristics resembling those of both Turing structures and standing waves. These patterns consist of regions separated by nodes at which the concentration is constant. Within each region, the concentration oscillates in time, but unlike a pure standing wave, where between each pair of nodes there is a single antinode with a maximum amplitude of local oscillation, these modulated standing waves display several antinodes in each region. The separation between nodes is equal to $\lambda_w/2$, while the spacing between antinodes is λ_T. Figures 3(a) and 3(b) show two examples of modulated standing waves. The system length L can fit 2 standing waves and 16 Turing wavelengths. The difference in appearance results from a phase shift between the standing wave and Turing modes. In Fig. 3(a) the standing wave nodes coincide with the minima of the shorter-wavelength Turing structures, while in the latter case these nodes occur at the

Turing structures' maxima. In the former case, the modulation is relatively weak [Fig. 3(a)], while coincidence of the maxima of one mode with the minima of the other leads to much more pronounced modulation of the standing waves [Fig. 3(b)]. We have also obtained patterns that are combinations of those shown in Figs. 3(a) and 3(b).

For parameters well above the bifurcation lines in domain IV or VI, the dispersion curve contains two broad positive maxima. One-dimensional calculations reveal that the combination of Turing and wave instabilities can produce pinning of Turing structures combined with traveling waves [Fig. 3(c)]. These localized Turing structures, surrounded by domains of traveling waves, are analogous to patterns found in the vicinity of a codimension-two Hopf–Turing point.[11–13] The localized Turing-like structures display small oscillatory variations in time and become sources of traveling waves, which move in opposite directions, then collide and disappear at fixed ''sink'' locations.

In a short system ($L \leqslant \lambda_w$), the mixed-mode patterns arising from the Turing and wave instabilities are stable, while the pure mode patterns are unstable. We refer to mixed-mode patterns either as modulated Turing structures or as modulated standing waves, based on the dominant mode. When the length of the system is significantly larger than the wavelength corresponding to the wave instability ($L \geqslant 6\lambda_w$), the mixed-mode pattern loses stability, and spatiotemporal chaos develops.

We have also performed numerical investigations in two spatial dimensions and we again find mixed-mode patterns (Fig. 4). Fourier spectra of these patterns suggest the presence of two modes with very different wave numbers. Analogous mixed-mode patterns were reported in experiments on the chlorite-iodide-malonic acid (CIMA) reaction.[26] Although the authors suggest that the different modes in their experiments reside on different parallel planes in a three-dimensional medium, our study reveals that similar mixed-mode patterns can arise in a single plane in a two-dimensional system when Turing and wave instabilities interact. In contrast to the one-dimensional solutions, where for this set of parameters the mixed-mode pattern is stable, the modulation occurs in two dimensions only as a transient process. Even though this pattern can persist for many oscillation periods, the system always evolves into either hexagonal Turing structures or standing or traveling waves. Thus it appears that near the Turing-wave codimension-two bifurcation point the pure modes have a larger domain of stability in systems of higher dimensionality.

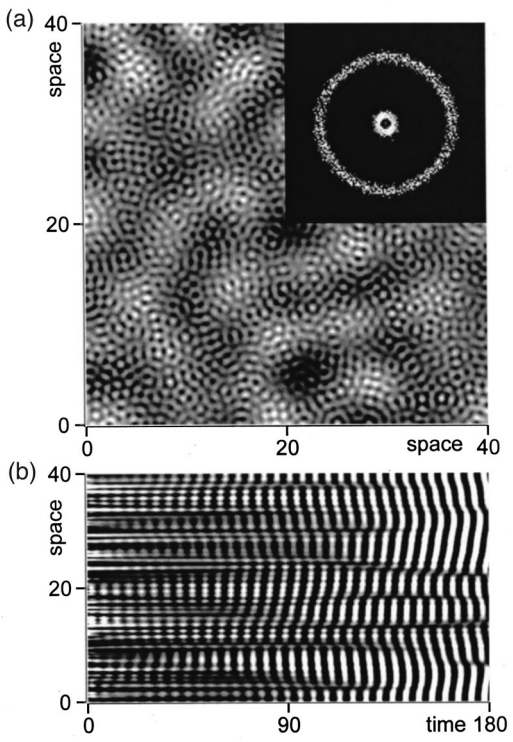

FIG. 4. A transient mixed-mode pattern with standing and traveling waves and Turing structures in a two-dimensional Brusselator system with zero-flux boundary conditions. Parameters: $(a,b)=(1.00,2.96)$, size of system 40×40. (a) Snapshot at $t=70$, inset shows Fourier spectrum with two characteristic frequencies. Short wavelength, represented by a large white circle, corresponds to Turing structures ($\lambda_T=0.96$ space unit); longer wavelength, represented by a small white circle, corresponds to traveling and/or standing waves ($\lambda_w=8.06$ space unit). (b) Pattern evolution from random initial conditions along the middle horizontal line.

IV. EXTENDED OREGONATOR MODEL

To see how the generic features of pattern formation arising from the interactions between Turing and wave instabilities might display themselves in a more realistic model of an oscillatory chemical reaction, we also analyzed the Oregonator model[24,25] of the BZ reaction, appending an additional reversible transition between the activator and its unreactive form in the same fashion as in the extended Brusselator model,

$$A+Y\xrightarrow{k_3}X+P, \tag{6}$$

$$X+Y\xrightarrow{k_2}2P, \tag{7}$$

$$A+X\xrightarrow{k_5}2X+2Z, \tag{8}$$

$$2X\xrightarrow{k_4}A+P, \tag{9}$$

$$B+Z\xrightarrow{k_c}\tfrac{1}{2}fY, \tag{10}$$

$$X\xrightarrow{k_\alpha}R, \tag{11}$$

$$R\xrightarrow{k_\beta}X, \tag{12}$$

where $A=[\mathrm{HBrO_3^-}]$, $B=$malonic acid, $P=$HOBr, $X=[\mathrm{HBrO_2}]$, $Y=[\mathrm{Br^-}]$, $Z=$oxidized form of catalyst, and R is the unreactive form of X. From the scheme (6)–(12), and using a quasisteady-state approximation for Y, a three-variable reaction-diffusion model is obtained,

$$\frac{\partial x}{\partial \tau}=D_x\nabla^2 x+\frac{1}{\epsilon}\left(x-x^2-fz\frac{x-q}{x+q}-(cx-dr)\right), \tag{13}$$

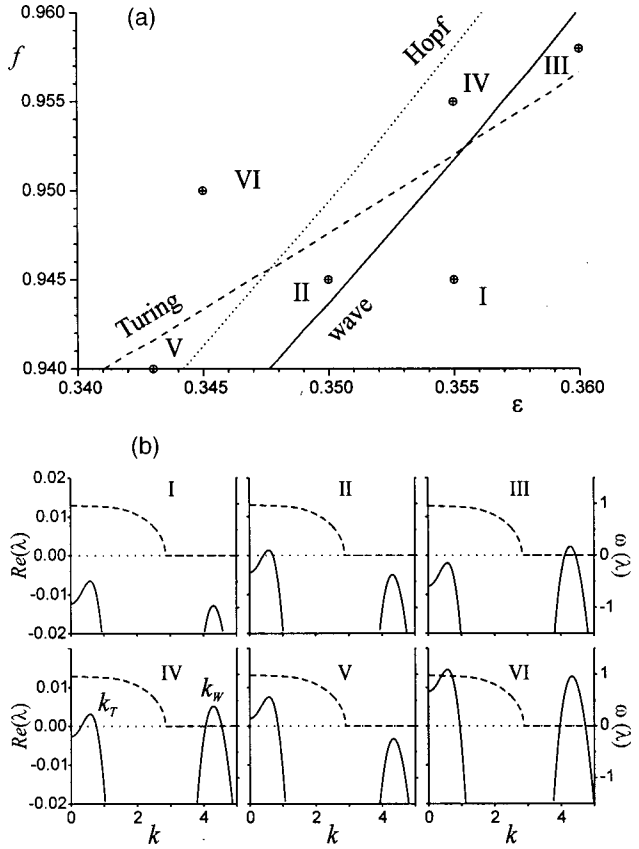

FIG. 5. Bifurcation diagram for the extended Oregonator model (13)–(15). Three bifurcation lines separate the parameter space into six domains (a) with dispersion relations shown in (b). Parameters $(D_x, D_z, D_r) = (0.025, 0.12, 0.8)$, $c = 0.2$, $d = 1$, $\epsilon_1 = 2$, and $q = 0.009$, $(\epsilon, f) = (0.355, 0.945)$ (I); $(0.350, 0.945)$ (II); $(0.360, 0.958)$ (III); $(0.355, 0.955)$ (IV); $(0.343, 0.940)$ (V); and $(0.345, 0.950)$ (VI). Solid line: real part of the most positive eigenvalue; dashed line: imaginary part of the complex pair of eigenvalues.

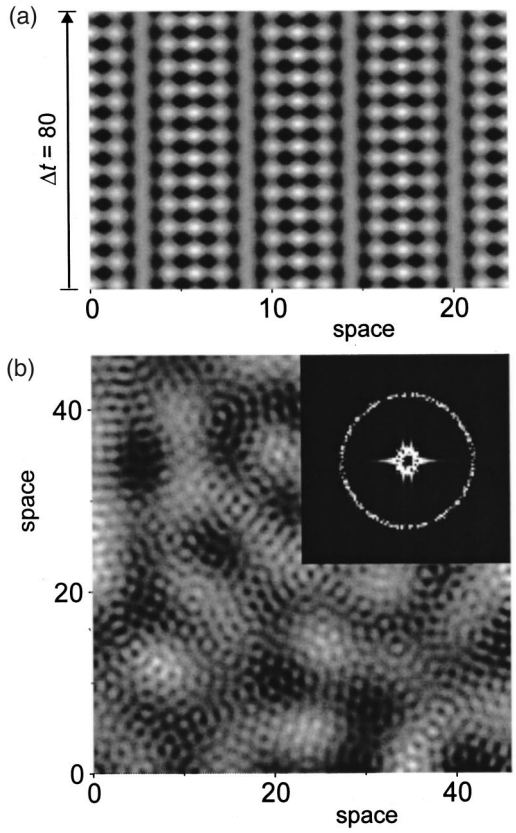

FIG. 6. Pattern formation near the codimension-2 Turing-wave point in the extended Oregonator model. Parameters are as in Fig. 5(b), IV. (a) 1-D modulated standing waves. (b) 2-D transient mixed-mode patterns.

$$\frac{\partial z}{\partial \tau} = D_z \nabla^2 z + x - z, \tag{14}$$

$$\frac{\partial r}{\partial \tau} = D_r \nabla^2 r + \frac{1}{\epsilon_1}(cx - dr), \tag{15}$$

where variables x, z, r are the nondimensionalized concentrations of species X, Z, R, respectively, and parameters ϵ, ϵ_1, q, c, d are rescaled kinetic parameters.

Linear stability analysis is also applied to the extended Oregonator model. The steady-state solution is at $x_{ss} = z_{ss} = (1 - q - f + \sqrt{1 - 2f + 2q + f^2 + 6fq + q^2})/2$, and $r_{ss} = x_{ss} c/d$. Figure 5 shows a bifurcation diagram with the Hopf, Turing and wave bifurcation lines. This diagram is similar to that shown in Fig. 1 for the extended Brusselator model.

One-dimensional solutions of this extended Oregonator model reveal pattern formation analogous to that obtained for the extended Brusselator model. Turing structures are stable in the pure Turing instability domain III, and standing waves are stable in the pure wave instability domain II. In domain IV the Turing and wave instabilities coexist. The interaction or competition between them results in formation of mixed-mode patterns. When the parameters of the system are selected close to the codimension-two Turing-wave point, stable spatially resonant mixed-mode patterns may form. As in the extended Brusselator model, these resonant patterns are only stable in a one-dimensional (1-D) system [Fig. 6(a); cf. Fig. 3(b)]. We did not obtain resonant patterns in two dimensions. The 2-D mixed-mode patterns [Fig. 6(b)] only appear as transients, and they usually transform into Turing structures or traveling waves.

In domain VI, all three instabilities coexist, and the pattern formation in this domain is more complex. Turing structures and traveling waves (primarily spiral waves) represent two types of patterns that may arise in this domain. The combination of these patterns leads to the formation of interesting mixed-mode patterns. The calculations presented in Fig. 7 were started from the steady state with a small random initial perturbation. The Turing mode quickly grows, and depending on the parameter f, hexagonal spots [Fig. 7(a)], labyrinthine stripes [Fig. 7(b)], or honeycomb spots [Fig. 7(c)] develop. However, the Turing structures do not occupy the entire medium, and there are several ''holes'' without Turing structures, which display oscillation due to the Hopf instability. A similar pattern of Turing structures with ''Hopf holes'' has been observed experimentally in the CIMA reaction.[26] During the pattern evolution, the ''Hopf holes'' become larger, and phase waves appear within them. The phase waves grow and develop curvature, typically evolving into spiral or target waves, which gradually spread into the area occupied originally by the Turing structures [the last frames

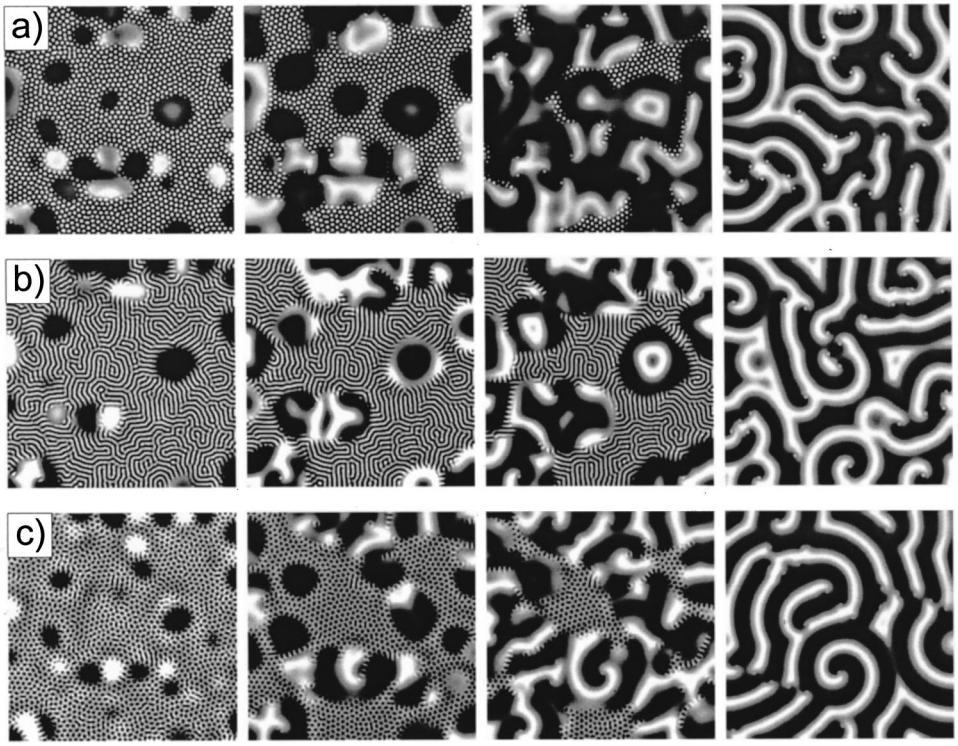

FIG. 7. The formation of antispiral waves and antitarget patterns from Turing structures in the domain of coexisting Turing, Hopf, and wave instabilities. Numerical solutions of the extended Oregonator model (13)–(15). Size: 64×64. Parameters: $\epsilon=0.32$, other parameters (except f) as in Fig. 5. Transient Turing structures contain (a) hexagonal spots ($f=1.1$), snapshots at $t=120$, 200, 340, 3000 time units; (b) labyrinthine stripes ($f=1.0$), snapshots at $t=160$, 280, 380, 1100 time units; and (c) honeycomb spots ($f=0.95$), snapshots at $t=120$, 300, 460, 6180 time units.

of Figs. 7(a)–7(c)]. Eventually, only several isolated Turing spots remain as the tips of spirals. The spiral interaction is a long-term process due to this ''pinning effect.'' These pinned spirals [the last frames of Figs. 7(a)–7(c)] in the extended Oregonator model are analogous to the 1-D results for the extended Brusselator model presented in Fig. 3(c).

The traveling waves shown in Fig. 7 are inwardly propagating (IP) waves, which move toward the target center (antitargets) or toward the tips of spirals (antispirals). Both antitarget and antispiral waves have been observed in the BZ-AOT system.[22] Although the spontaneous formation of IP waves can occur in domain VI, where the Hopf, Turing, and wave instabilities coexist, the Turing and Hopf instabilities are not necessary conditions for IP waves to occur. The wave instability and negative group velocity [$d\omega/dk<0$; see the dispersion curves in Fig. 5(b)] suffice to generate IP waves. We illustrate this point in Fig. 8, where we show the spontaneous formation of antispiral and antitarget patterns in the pure wave instability domain [see Fig. 5(b)(II)], for a negative group velocity, $v_g=-0.025$ at wave number $k=0.575$.

V. DISCUSSION AND CONCLUSION

In this study we focus on pattern formation arising from the interaction between Turing and wave instabilities. The Turing instability appears when the inhibitor diffuses faster than the activator; the wave instability requires that the unreactive form of the activator diffuse even faster than the inhibitor in our three-variable models.

Two different models, the Brusselator and the Oregonator, are explored in this study. The former includes a cubic autocatalytic term, the latter does not. Even though they have very different kinetics (and thus the shapes of their nullclines differ), they produce very similar results. In the vicinity of the codimension-2 Turing-wave bifurcation point, mixed-mode patterns are stable in 1-D systems when spatial resonance occurs. Spatial resonance is essential for the stability of these mixed-mode patterns. Far from the codimension-2 point, patterns consisting of combinations of Turing structures and traveling waves arise as dense ''pinned'' spirals. Antispirals arise in both models when the group velocity is negative.

The patterns reported here may arise in any system with

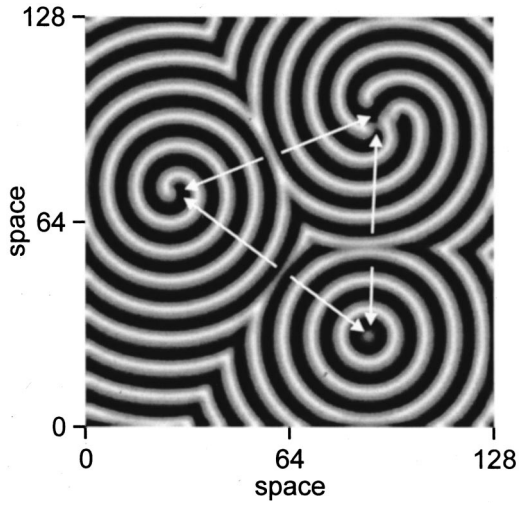

FIG. 8. Spontaneous formation of antispiral and antitarget waves with negative group velocity in the domain of pure wave instability. An extended Oregonator model with parameters: $(\epsilon,f)=(0.325,0.910)$; all other parameters as in Fig. 5. A small random perturbation is applied at $t=0$. A snapshot is taken at $t=100\,000$ time units. There are one four-arm and one one-arm antispiral and one antitarget pattern. Arrows indicate the directions of wave propagation.

coexisting Turing and wave modes. The introduction of an unreactive, rapidly diffusing form of an autocatalytic species is one way to achieve this in a reaction-diffusion system subject to Turing instability. Such conditions may occur in chemical systems (e.g., in microemulsions[22]) or, more significantly, in biological cells, where the existence of a multiphase environment, molecules with a wide range of molecular weights, and the possibility of one- and two- as well as three-dimensional diffusion make this sort of behavior feasible.

ACKNOWLEDGMENT

This work was supported by the Chemistry Division of the National Science Foundation.

[1] M. C. Cross and P. C. Hohenberg, Rev. Mod. Phys. **65**, 851 (1993).
[2] I. R. Epstein and J. A. Pojman, *An Introduction to Nonlinear Chemical Dynamics* (Oxford University Press, New York, 1998).
[3] H. L. Swinney and V. I. Krinsky, in *Waves and Patterns in Chemical and Biological Media*, Physica D **49**, 1 (1991).
[4] R. Kapral and K. Showalter, in *Chemical Waves and Patterns* (Kluwer, Dordrecht, 1995).
[5] A. M. Turing, Philos. Trans. R. Soc. London, Ser. B **237**, 37 (1952).
[6] V. Castets, E. Dulos, J. Boissonade, and P. De Kepper, Phys. Rev. Lett. **64**, 2953 (1990).
[7] D. Walgraef, *Spatio-Temporal Pattern Formation* (Springer-Verlag, Berlin, 1997).
[8] M. Hildebrand, A. S. Mikhailov, and G. Ertl, Phys. Rev. Lett. **81**, 2602 (1998).
[9] A. M. Zhabotinsky, M. Dolnik, and I. R. Epstein, J. Chem. Phys. **103**, 10306 (1995).
[10] M. Dolnik, A. M. Zhabotinsky, A. B. Rovinsky, and I. R. Epstein, J. Phys. Chem. A **103**, 38 (1999); M. Dolnik, A. B. Rovinsky, A. M. Zhabotinsky, and I. R. Epstein, Chem. Eng. Sci. **55**, 223 (2000).
[11] J.-J. Perraud, A. De Wit, E. Dulos, P. De Kepper, G. Dewel, and P. Borckmans, Phys. Rev. Lett. **71**, 1272 (1993).
[12] A. De Wit, D. Lima, G. Dewel, and P. Borckmans, Phys. Rev. E **54**, 261 (1996).
[13] M. Meixner, A. De Wit, S. Bose, and E. Schöll, Phys. Rev. E **55**, 6690 (1997); S. Bose, P. Rodin, and E. Schöll, *ibid.* **62**, 1778 (2000).
[14] M. C. Cross, Phys. Rev. Lett. **57**, 2935 (1986).
[15] S. Jakubith, H. H. Rotermund, W. Engel, A. v. Oertzen, and G. Ertl, Phys. Rev. Lett. **65**, 3013 (1990).
[16] O. Lev, M. Sheintuch, L. M. Pisemen, and C. Yanitzky, Nature (London) **336**, 458 (1988).
[17] G. A. Cordonier, F. Schuth, and L. D. Schmidt, J. Chem. Phys. **91**, 5374 (1989).
[18] G. Philippou, F. Schultz, and D. Luss, J. Phys. Chem. **95**, 3224 (1991).
[19] P. Strasser, J. Christoph, W.-F. Lin, M. Eiswirth, and J. L. Hudson, J. Phys. Chem. A **104**, 1854 (2000).
[20] A. v. Oertzen, H. H. Rotermund, A. S. Mikhailov, and G. Ertl, J. Phys. Chem. A **104**, 3155 (2000).
[21] N. Mazouz and K. Krischer, J. Phys. Chem. B **104**, 6081 (2000); K. Krischer, N. Mazouz, and G. Flätgen, *ibid.* **104**, 7545 (2000).
[22] V. K. Vanag and I. R. Epstein, Science **294**, 835 (2001); Phys. Rev. Lett. **87**, 228301 (2001).
[23] I. Prigogine and R. Lefever, J. Chem. Phys. **48**, 1695 (1968).
[24] R. J. Field and R. M. Noyes, J. Chem. Phys. **60**, 1877 (1974).
[25] J. P. Keener and J. J. Tyson, Physica D **21**, 307 (1986).
[26] J. Boissonade, E. Dulos, and P. De Kepper, in *Chemical Waves and Patterns*, edited by R. Kapral and K. Showalter (Kluwer, Dordrecht, 1995), p. 221.